Proceedings of FUELCELL2006
Fourth International Conference on Fuel Cell Science, Engineering and Technology
June 19-21, 2006, Irvine, California USA

FUELCELL2006-97075

ORDER REDUCTION FOR A CONTROL-ORIENTED MODEL OF THE WATER DYNAMICS IN FUEL CELLS

B. A. McCain[*]
Fuel Cell Control Laboratory
Department of Mechanical Engineering
University of Michigan, Ann Arbor, MI 48109
and the
Toyota Technical Center, USA
Powertrain Division, Ann Arbor, MI, 48105
Email: bmccain@umich.edu

A. G. Stefanopoulou[†]
Fuel Cell Control Laboratory
Department of Mechanical Engineering
University of Michigan, Ann Arbor, MI 48109
Email: annastef@umich.edu

ABSTRACT

Predicting the water dynamics and estimating humidity and flooding conditions in a low-temperature fuel cell are critical for robust operation and long life. Previous work by McKay et al [1] shows that the fuel cell anode, cathode, and membrane water dynamics and gaseous species concentrations can be accurately modeled by discretizing the partial differential equations that describe mass transport into three segments. Avoiding sensitivities associated with over-parameterization, and allowing for the real-time computations necessary for embedded controllers, requires in-depth investigation of the model order.

In this paper the model from [1] is formulated into a bond graph representation. The objective is to establish the necessary model order for the fuel cell model using the Model Order Reduction Algorithm (MORA) [2], where an energy-based metric termed the *Activity* is used to quantify the contribution of each element of the model. *Activity* is a scalar quantity that is determined from the generalized *effort* and *flow* through each element of the model. We show the degree of model order reduction and provide a guideline for appropriate discretization.

[*]Supported by Toyota Technical Center, USA, Inc
[†]Work supported by the National Science Foundation (NSF) CMS-0201332 and CMS-0219623

1 Introduction

The management of water within the fuel cell stack is critical for optimal stack performance. A balance must be struck between hydrogen and oxygen delivery, and water supply (removal). Water will condense when the reactant gases become saturated. This liquid water can accumulate in the gas channels and/or the pore space of the gas diffusion layer (GDL), and can partially coat the catalyst, reducing the power output of the fuel cell.

Computational fluid dynamics models have been developed to approximate the 2 or 3 dimensional flow of hydrogen, air, and water within the manifolds, gas channels, and the gas diffusion layers [3–6]. While these models are suitable for investigating fuel cell design issues, implementation of such complex models for real time embedded control is cumbersome. Thus, any model-based control scheme used for water management must adequately obtain implementation feasibility while still capturing the dynamic behavior of electrode flooding and two phase flow.

In this paper, we investigate the necessary model fidelity to accurately predict flooding of a fuel cell stack. The work of McKay et al [1] showed that spatial discretization can be used to approximate a fuel cell system described by partial differential equations. In the discrete model, the GDL of both cathode and anode sides were divided mathematically into three sections. The spatial characteristics (temperature, composition, pressure)

of each section are considered to be homogeneous.

The premise for the discretization in [1] is that the inclusion of equations describing liquid water and gas dynamics within the GDL is necessary to predict flooding. The question we study in this paper is if this is true for all gas species and the liquid water, and if three sections is the most appropriate resolution.

While the three-section discretization has adequate prediction capability, and is not overly complex, the model still has 25 states. In order to pursue model-based control of this system, it would be beneficial to reduce the model order further to permit online parameter identification and adaptation while controlling the system in real time.

In this paper, a model order reduction methodology developed by Stein and Louca [2], combined with the appropriate modeling tool known as bond graphs, is utilized in an application to reduce the order of the discretized fuel cell model described in [1].

2 Nomenclature

This section describes the naming conventions used in this paper. Time derivatives will be written as $d(\,)/dt$. Spatial derivatives through the GDL thickness in the direction normal (y) to the membrane are denoted as $\partial(\,)/\partial y$.

A_{fc} is the fuel cell active area (m^2), c is molar concentration (mol/m^3), D is the diffusion coefficient (m^2/s), D_{eff} is the effective diffusivity (m^2/s), i is current density (A/cm^2), I_{st} is the stack current (A), M is molecular weight (kg/mol), n is the molar flow rate (mol/s), p is pressure (Pa), R is the ideal gas constant (J/kg K), r_v is the water evaporation rate ($mol/m^3/s$), s is the fraction of liquid water volume to the total pore volume, S is the reduced water saturation, T is temperature (K), V is volume (m^3), and Q represents liquid volumetric flow rate (m^3/s).

For the bond graph-related terms, $\mathbf{e}(t)$ will represent the *effort*, with $\mathbf{f}(t)$ for the *flow*, both of which vary with time. R and C will represent the general concepts of *resistance* and *capacitance*, respectively. An M preceding an R will indicate that the resistance is modulated, and the modulus will be defined locally.

The Greek letter α_w is the tunable diffusion parameter, γ is used for the volumetric condensation coefficient (s^{-1}), ε for porosity, ρ for density (kg/m^3).

The subscript *an* denotes variables associated with the anode, *c* is capillary, *ca* is cathode, *ch* is channel, *ct* is catalyst, *e* is electrode (*an* or *ca*), H_2 is hydrogen, N_2 is nitrogen, O_2 is oxygen, *mb* indicates an assignment to the cell membrane, *j* is used as an index for fuel cell constituents, *k* is used as an index for discretization, *l* is liquid, *p* is pore, *rct* is reactions, *sat* is saturation, and *v* is vapor.

3 Model Order Reduction Algorithm

As explained in detail in [2], the Model Order Reduction Algorithm is a method that seeks to simplify complex models by creating a metric the authors named *Activity* to determine the energetic contribution of every element of a model. Starting from the concept of $Power = P = effort \cdot flow$, the *Activity* is defined:

$$Activity_j = \int_0^T |P_j(t)|dt = \int_0^T |\mathbf{e}_j \cdot \mathbf{f}_j|\, dt. \qquad (1)$$

As can be seen from (1), it is necessary to assign a time duration for the *Activity* calculation. This is a critical aspect of the method, as results will vary depending upon this time range.

Once the *Activity* of an element is determined, it is normalized by an *Activity Index*(AI) to determine whether the element has significant contribution to the overall energy of the system. The definition of the *Activity Index*(AI) is:

$$AI_j = \frac{Activity_j}{\sum_1^m (Activity_i)}, \qquad (2)$$

where m is the total number of energetic (energy-utilizing) elements in the model.

As a function of the sum total of all the individual element *Activites*, the *AI* provides a means to compare elements from any part of the model.

An important aspect of the MORA is that it reduces model complexity while maintaining the physical meaning of the variables and parameters. It is also applicable to nonlinear systems, which, due to the highly nonlinear nature of this model, makes it attractive for use here.

4 Model Overview

On the anode side of the fuel cell, a mixture of hydrogen and water vapor flows from the channel through the GDL. A mixture of oxygen, nitrogen, and water vapor flows from the cathode channel. The species concentrations in the channels are calculated assuming the channel is homogeneous, lumped-parameter, and isothermal. The time varying channel concentrations provide one set of boundary conditions for the spatially varying reactant concentrations within the GDL. The reactant gases must diffuse through the GDL to reach the catalytic layer.

Under load, it is assumed that product water is formed as a vapor at the cathode catalyst. The combination of electro-osmotic drag and back-diffusion transport vapor through the membrane between the anode and cathode. The net molar flow of vapor through the membrane depends on the relative magnitudes of back-diffusion and drag.

The flow chart of Fig.1 pictorially describes the interrelationships between the gas concentrations/flows, the capillary-pressure-driven liquid water flow, the influence of liquid water volume, the chemical reactions, and the voltage output. A key aspect to note is that the dynamic variable V_l affects both diffusion of gas species and the capillary pressure by way of the water saturation ratio ($s = \frac{V_l}{V_p}$) [7].

Under the isothermal conditions assumed for both anode and cathode GDL for this model, when the production or transport of vapor exceeds the ability of the vapor to diffuse through the

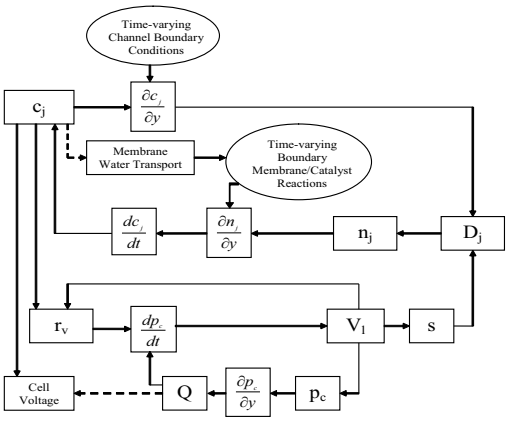

Figure 1. Flow chart of model calculation algorithm

GDL to the channel, the vapor supersaturates and condenses. The condensed liquid accumulates in the either or both the anode and cathode GDL until it has surpassed the immobile saturation threshold, at which point capillary flow will carry it to an area of lower capillary pressure (the GDL-channel interface). Liquid water in the GDL occupies pore space, reducing the effective area through which reactant gas can diffuse. This obstruction ultimately reduces the active catalyst surface area, in turn lowering the cell voltage.

4.1 Discretization

The mass transport of gas and liquid water is divided into discrete volumes (Fig. 2). The spatial gradients are solved as difference equations, while the time derivatives are solved with standard ODE solvers.

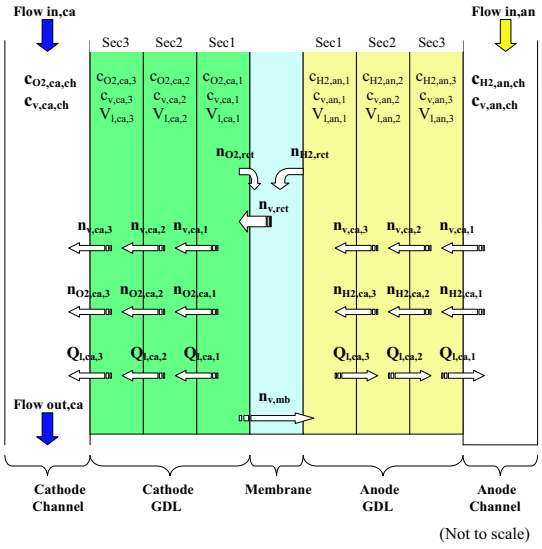

Figure 2. Mass transport diagram with discretization of diffusion layer

For the cathode, difference equations are used to describe the concentration of oxygen, c_{O_2}, vapor, $c_{v,ca}$, and reduced water saturation, S_{ca}. For the anode, difference equations are used to describe the concentration of hydrogen, c_{H_2}, vapor, $c_{v,an}$, and reduced water saturation, S_{an}.

As an example of a three-stage discretization of the O_2 and H_2 diffusion equations, the difference equations for the molar flow gradients of oxygen and hydrogen are:

Cathode Equations	Anode Equations
$\frac{\partial n_{O_2}}{\partial y}(1) = \frac{n_{O_2}(1) - n_{O_2,rct}}{\delta y}$	$\frac{\partial n_{H_2}}{\partial y}(1) = \frac{n_{H_2,rct} - n_{H_2}(1)}{\delta y}$
$\frac{\partial n_{O_2}}{\partial y}(2) = \frac{n_{O_2}(2) - n_{O_2}(1)}{\delta y}$	$\frac{\partial n_{H_2}}{\partial y}(2) = \frac{n_{H_2}(1) - n_{H_2}(2)}{\delta y}$
$\frac{\partial n_{O_2}}{\partial y}(3) = \frac{n_{O_2}(3) - n_{O_2}(2)}{\delta y}$	$\frac{\partial n_{H_2}}{\partial y}(3) = \frac{n_{H_2}(2) - n_{H_2}(3)}{\delta y}$

(3)

where $n_{O_2,rct}$ and $n_{H_2,rct}$ are calculated from:

$$n_{j,rct} = \frac{I_{st}}{2\xi F} \text{ with } \begin{cases} \xi = 1 \text{ for j} = H_2 \text{ or j} = v \\ \xi = 2 \text{ for j} = O_2 \end{cases} \quad (4)$$

and F is Faraday's constant.

5 Derivation of the Bond Graph Equations

Application of the MORA of [2] requires both an understanding of the model on an element-by-element basis and knowledge of the *effort* and *flow* of each element over time. A modeling tool that lends itself conveniently to *Activity* analysis is the bond graph. For bond graph implementation, each system equation must be cast in a form that is applicable to the building blocks of the bond graph.

In the discrete model of [1], there are equations of gas diffusion, gas concentration time rate of change, capillary pressure-driven liquid water flow, evaporation, chemical reactions, and a number of conditional and empirical equations governing membrane mass transport.

The derivation and background for the following physical model equations can be found in [1]. In this paper, the equations modeling the physical system are used as the *starting* point for the bond graph model creation. Each subsection in this section will explain how the bond graph for each model phenomenon is derived.

5.1 Gas Species Concentration (Capacitance Model)

The rate of change of molar concentration $(c_j = \frac{p_j}{RT})$ of gas species j is:

$$\frac{dc_{j,e}}{dt} = \frac{1}{A_{fc}} \frac{\partial n_{j,e}}{\partial y} + r_{j,e} \quad (5)$$

where e denotes the electrode (anode or cathode) and the species denoted by j correspond to the oxygen O_2 and vapor v from the cathode, and to the hydrogen H_2 and vapor v from the anode. The reaction term $r_{j,e}$ is zero for the oxygen and hydrogen cases, whereas for the vapor case it captures the evaporation rate $r_{j,e} = \gamma(p_{v,sat}/(RT) - c_{v,e})$, where $p_{v,sat}$ is the saturation vapor pressure.

In discrete form (5) is written:

$$\frac{dc_{j,e}(k)}{dt} = \frac{1}{\delta y A_{fc}}(n_{j,e}(k) - n_{j,e}(k-1)) + r_{j,e}, \qquad (6)$$

where (k) and (k-1) represent any two sequential sections of the discrete model.

As can be seen from (6), the rate of change of concentration $(mol/s/m^3)$ becomes a function of the difference in molar flows across the section boundaries for the particular gas species. Additionally, the local reaction (evaporation) rate $r_{j,e}$ is included for the water vapor model. The O_2 and H_2 reactions are calculated as molar flows (mol/s), and thus enter the equation through the across-boundary flow.

The bond graph constitutive law for a *capacitance* is:

$$\frac{d\mathbf{e}(k)}{dt} = \frac{1}{C}(\mathbf{f}(k) - \mathbf{f}(k-1) + \mathrm{MSf}_{\mathrm{rct}}), \qquad (7)$$

where for our case $C = \delta y A_{fc} = V_p$ (the pore volume for one section), $\mathrm{MSf}_{\mathrm{rct}}$ is a modulated flow source that can represent a variety of flow inputs, but is non-zero for this application only when j is water vapor, *v*. From these observations, a choice of molar flow as the *flow* variable, concentration as the *effort* variable, and section volume for the *capacitance* for the gas mass transport is logical, and preserves physical meaning.

5.2 Gas Species Diffusion (Resistance Model)

Diffusion of gases takes place in the anode and cathode gas diffusion layers. On the anode side, relative diffusion of hydrogen and vapor must be considered, while the cathode side model must take into account the relative diffusion of oxygen, nitrogen, and vapor. This model is simplified by assuming that the presence of N_2 in the mixture does not significantly affect the diffusivity of O_2 and vapor.

The diffusion of gas species in the diffusion layer is a function of the concentration gradient, transferring gas from regions of higher concentration to regions of lower concentration:

$$n_{j,e} = -D_{j,eff} A_{fc} \frac{\partial c_{j,e}}{\partial y}. \qquad (8)$$

As shown in (8), the molar flow, $n_{j,e}$ (mol/s), depends on a diffusion coefficient, $D_{j,eff}$.

The discrete version of (8) is realized with $n_{j,e}$ being a function of the difference in the concentration between neighboring sections:

$$n_{j,e}(k) = \frac{-D_{j,eff} A_{fc}}{\delta y}(c_{j,e}(k) - c_{j,e}(k-1)) \qquad (9)$$

where $\delta y = (t_{GDL}/3)$ is the thickness of one section.

The general *resistance* constitutive law utilized in bond graphs is:

$$\mathbf{f}(k) = \frac{1}{R(k)}(\mathbf{e}(k) - \mathbf{e}(k-1)) \qquad (10)$$

where for this application the flow resistance is represented by a modulated resistance:

$$R(k) = MR(k) = \frac{\delta y}{D_{j,eff} A_{fc}}. \qquad (11)$$

A *modulated resistance* is necessary because the diffusivity of gas constituents in the GDL is affected by the volume of liquid water present, $V_{l,e}$, giving rise to an *effective* diffusivity [7]:

$$D_{j,eff}(k) = D_j \varepsilon \left(\frac{\varepsilon - 0.11}{1 - 0.11}\right)^{0.785} (1 - s_e(k))^2, \qquad (12)$$

where $s_e(k) = \frac{V_{l,e}(k)}{V_p}$, D_j is the diffusivity constant for the species j (which is dependent upon the molecular size of j), and V_p is the pore volume of one section of the diffusion layer [7].

5.3 Liquid Water Storage (Capacitance Model)

This water dynamics model was created on the hypothesis that liquid water may accumulate in both the anode and cathode GDL, and subsequently flow into the respective channels.

The volume of liquid water ($V_{l,e}$) in each GDL section is determined by the capillary liquid water volumetric flow rate, $Q_{l,e}$, and the evaporation rate, $r_{v,e}$:

$$\frac{dV_{l,e}}{dt} = Q_{l,e,in} - Q_{l,e,out} - \frac{r_{v,e} V_p M_v}{\rho_l} \qquad (13)$$

where the evaporation (condensation) rate governs the creation of liquid water micro-droplets (considered to be evenly distributed throughout the porous GDL), and where conditions necessary for water droplet formation are assumed to have been met [7]. For simplification of the model, dynamics associated with the formation of the liquid water droplets have been neglected.

In order to cast our model into a form that is conducive to calculation of "power equals the product of *effort* and *flow*", the time rate of change of liquid water volume should be translated into a dynamic capillary pressure relationship with volumetric flow.

As a pore fills with liquid water, the capillary pressure increases, causing the water to flow to an adjacent pore with less water. This process creates a flow of liquid water through the GDL, finally resulting in the incursion of liquid into the channel (shown in Fig. 3 [7]). Capillary pressure results from surface tension of the water droplets, and is calculated as follows:

$$p_{c,e} = \beta_{pc} g_{NL}(V_{l,e}), \qquad (14)$$

where β_{pc} is a constant that captures the geometry of the surface tension between the water and air, the porosity, and the permeability of the GDL. The nonlinear function $g_{NL}(V_{l,e})$ is a third-order polynomial in $V_{l,e}$ that describes the relationship between capillary pressure and the amount of liquid water present.

In this model, gravitational effects on the liquid water are considered negligible due to the liquid water surface tension interaction within the fibers of the GDL.

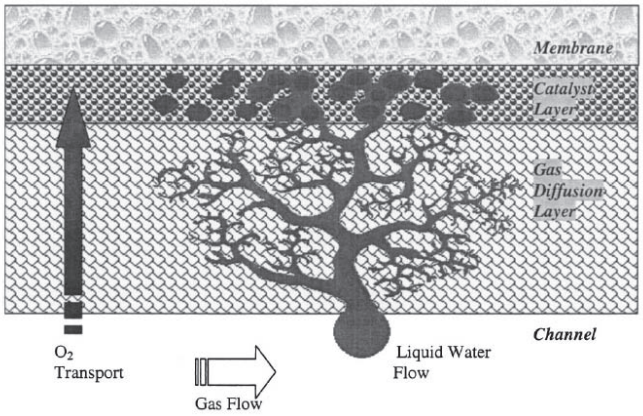

Figure 3. Capillary flow of liquid water through diffusion layer [7]

Taking the time derivative of (14), it can be shown that the time rate of change of the capillary pressure is related to the volumetric flow by a discrete equation of the form:

$$\frac{dp_{c,e}(k)}{dt} = \beta_Q g'_{NL}(V_{l,e},k)(Q_{l,e}(k) - Q_{l,e}(k-1) - r_{l,e}(k)), \quad (15)$$

where β_Q represents a constant that depends upon surface tension, permeability, and GDL porosity. The nonlinear function $g'_{NL}(V_{l,e},k)$ is the derivative of $g_{NL}(V_{l,e},k)$ from (14) with respect to $V_{l,e}$, and relates how capillary pressure varies with the volume of liquid water present. Further, the condensation rate $r_{l,e}$ is a conversion from $r_{v,e}$ to get appropriate units (m^3/s)(18).

Following the pattern of the previous subsections, the next step is to translate (15) into a bond graph compatible form. While (15) could be implemented using a modulated capacitance, simulations have shown that a simplification can be obtained by using the mean value for the applicable range of $g'_{NL}(V_{l,e})$. This direction is justified by noting first that per [7], our model assumes no liquid water flow until 10% of the pore volume is filled with liquid water. At that point capillary action causes the liquid to flow into the next section, significantly reducing the liquid water fill rate for the original section, while notably increasing the fill rate for the next. The practical range of $V_{l,e}$ is small enough after liquid flow begins to justify use of the mean value, therefore $g'_{NL}(V_{l,e},k)$ becomes $\bar{g}$.

Then, with the evaporation modeled as a modulated flow source, the capillary pressure equation can now be modeled as a *capacitance* in a bond graph model:

$$\frac{d\mathbf{e}(k)}{dt} = \frac{1}{C}(\mathbf{f}(k) - \mathbf{f}(k-1) - \mathrm{MSf}_r). \quad (16)$$

Where the *capacitance* becomes:

$$\frac{1}{C} = \beta_Q \bar{g} \quad (17)$$

and the molar liquid evaporation rate is represented by a modulated flow source:

$$MSf_r = r_{l,e} = \frac{M_v V_p}{\rho_l} r_{v,e}. \quad (18)$$

5.4 Liquid Water Transport (Resistance Model)

The remaining equation to be modeled in bond graph form is the liquid water flow. Parameters that affect the mass flow rate of liquid water are flow area, permeability, viscosity and density of liquid water, and the section thickness. These factors will naturally influence the resistance to flow for this element. It is, however, the presence of a liquid water volume gradient that drives the liquid water flow. Capillary pressure and liquid water volume are related through (14).

The physics of the liquid flow phenomenon are described by:

$$Q_{l,e} = \beta_{wl} S_e^3 \left(\frac{\partial p_{c,e}}{\partial y}\right), \quad (19)$$

where $p_{c,e}$ is capillary pressure, $S_e = 1.1\left(\frac{V_{l,e}}{V_p} - 0.1\right)$ is the reduced water saturation, β_{wl} is a constant that embodies flow area, permeability, density, and viscosity, and $\partial p_{c,e}/\partial y$ describes the influence spatial variation of capillary pressure has on volumetric flow rate.

Similar to the gas species diffusion bond graph equation, an application of a *modulated resistance*, in discrete form, is appropriate:

$$\mathbf{f}(k) = \frac{1}{MR(k)}(\mathbf{e}(k) - \mathbf{e}(k-1)). \quad (20)$$

In the bond graph model, the *MR* will be a function of several system parameters (listed below in the explanation of β_R), and the continuously varying liquid water volume:

$$\frac{1}{MR(k)} = \beta_R S_e^3, \quad (21)$$

where β_R is a constant that depends upon flow area, permeability, water viscosity, section thickness and porosity, and surface tension. The volumetric flow rate is calculated from:

$$Q_{l,e}(k) = \frac{1}{MR(k)}(p_{c,e}(k) - p_{c,e}(k-1)). \quad (22)$$

Capillary pressure as the *effort* variable and volumetric flow rate as the *flow* variable were natural choices, as was the liquid water volume as the modulus.

Finally, a conditional statement must be included to prevent capillary action from starting unless the liquid water volume reaches 10% of the pore volume (the minimum condition for flow suggested in [7]).

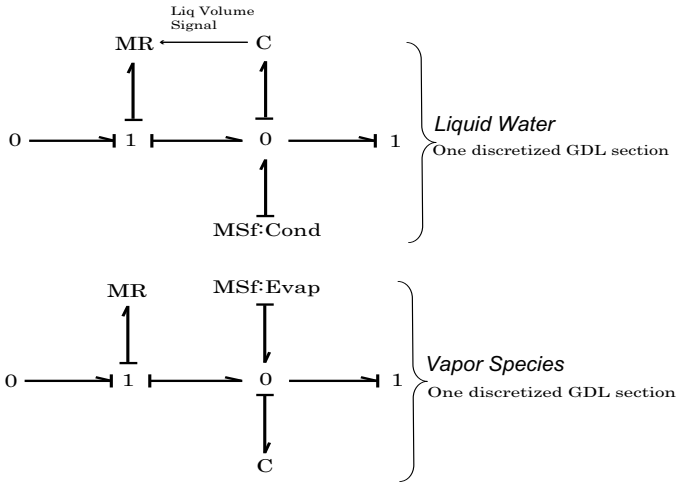

Figure 4. Bond Graph Building Block for one Discrete GDL Section

6 The Bond Graph Model

The goal of this model order reduction is to determine the minimum number of sections required to accurately model flooding. Therefore, a repeatable bond graph model for one section would be useful.

Using the relationships from Section 5, a single section bond graph "submodel" was created (Fig. 4). With this submodel, a GDL discretization for a range of resolutions can be easily accomplished.

6.1 Boundary Conditions

Flow through the GDL is bounded on one side by the channel, and on the other by the catalyst-coated membrane. These boundary conditions are clarified in this section.

The conditional and empirical equations for the membrane water transport do not fit into standard bond graph form, so function blocks were built to accommodate them. The air, hydrogen and water vapor supplied to the gas distribution channels are easily modeled as flow sources, where the amount supplied can be controlled to supply the desired O_2 and H_2 excess ratios. Similarly, evaporation is modeled as a modulated flow source, with presence of liquid water as the fundamental prerequisite and the modulus being the product of the evaporation coefficient and water vapor pressure relative to the saturation pressure.

The concentration of reactants and vapor in the anode and cathode channels are used for calculation of the gas concentration gradient in the last GDL layer (next to the channel). The masses of gas species in the channels are balanced by applying mass continuity. The channel species concentrations are calculated from pressures determined using Dalton's law of partial pressure. The boundary values for the liquid water saturation at the GDL-channel interface are set to zero due to the hydrophobicity of the GDL material. The boundary conditions for the gas compositions at the GDL-channel interface are set equal to the channel compositions ($c_{j,e,ch}$), which in turn depend on the inlet flow and vapor composition, which depend on controllable inputs.

The boundary conditions for the molar flow at the GDL-catalyst interface are equal to the chemical reaction rates and the membrane water transport, which in turn depend on the GDL species concentrations at the catalyst $c_{j,e,ct}$ and the current drawn from the stack I_{st} (4)(23). The molar flow $n_{v,mb}$ of vapor across the membrane is calculated using mass transport principles and membrane properties proposed in [8]:

$$n_{v,mb} = d_o \frac{i}{F} - \alpha_w A_{fc} D_w \frac{(c_{v,ca,ct} - c_{v,an,ct})}{t_{mb}}, \qquad (23)$$

where i is the fuel cell current density (I_{st}/A_{fc}), the osmotic drag coefficient, d_o, is used to calculate the vapor molar flow from the anode to the cathode due to electro-osmosis, D_w is used to calculate the diffused vapor molar flow from the cathode to the anode due to the water concentration gradient in the membrane boundary through Fick's law, and t_{mb} is the membrane thickness. The parameter α_w is the only modification to the model in [8] and was identified through experiments.

The electro-osmotic drag coefficient (d_o) and water diffusivity (D_w) through the membrane are functions of λ_{mb}, the membrane water content, which is a function of the vapor concentrations on each side of the membrane [8] [5].

Stacking three of the discretized sections from Fig. 4 for each constituent of interest, including function submodels for the membrane physics, adding evaporation flow sources, and putting in flow sources for the supply of air and hydrogen gives the model shown in Fig. 5. In this full bond graph model, the channels are modeled as dynamic boundary conditions and shown on the far left and right sides of the bond graph. The flow into and out of the fuel cell occurs in the channels. The cathode side of the model is the left half of the model, the anode side the right half. The membrane is located in the middle of the model. Positive flow in the model is defined to be from anode channel to cathode channel.

Finally, for the purpose of model simplification, the concentration of nitrogen throughout the cathode diffusion layer is assumed to be identical to the concentration in the channel.

6.2 Effect of Flooding on Current Density

Once anode flooding occurs, the authors of [1] postulate that the resulting voltage degradation arises from the accumulation of liquid in the GDL, $V_{l,e}$. The accumulated liquid mass is assumed to form a film of thickness t_{wl}, blocking part of the active fuel cell area A_{fc} and consequently increasing the lumped current density, defined as apparent current density i_{app}:

$$i_{app} = I_{st}/A_{app} \qquad (24)$$

where the apparent fuel cell area A_{app} is approximated as

$$A_{app} = (A_{fc} - V_{l,an}/t_{wl}) \, . \qquad (25)$$

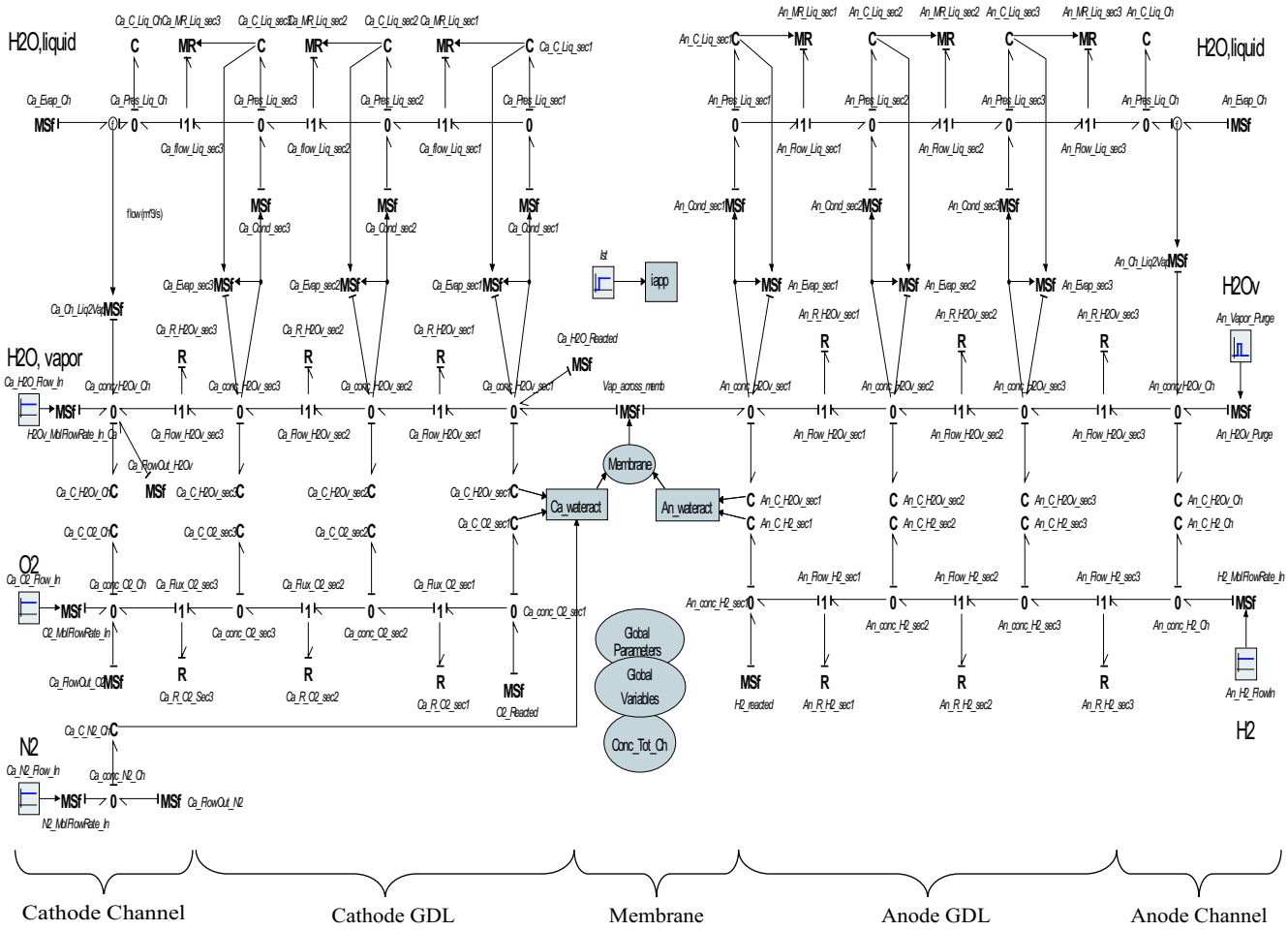

Figure 5. Complete Bond Graph Representation of a 3-Section Discrete Water Dynamics Model

7 Data and Analysis

Even with the assumption of isothermal conditions, the 3-section discrete model [1] accurately captures the water dynamics of a stack current increase, the cell voltage resulting from a temperature increase, and the cell voltage degradation over time as liquid water builds.

This model was verified using a 24-cell PEMFC stack capable of delivering 1.4 kW of continuous power, and a peak output of 2.5 kW. The gas is distributed from the machined graphite flow fields through double-sided, hydrophobic version 3 $ETek^{TM}$ Elats with a thickness of 0.432 mm. The catalyst-coated membrane has a surface area of approximately 300 cm^2 [1].

Experiments performed at moderate temperatures (60 ^oC) and current densities (less than 0.5 A/cm^2), with dry hydrogen supply, indicate that back-diffusion dominates electro-osmotic drag, resulting in a net transport of vapor across the membrane from cathode to anode. Subsequent purge events of the dead-ended anode channel revealed flooding. Following the anode purge, the voltage from the stack dramatically improved. Further, under similar conditions, surging the cathode had little effect on voltage. Based upon these observations, it was decided to focus on anode flooding prediction as the key to modeling voltage degradation [1].

Figure 6 shows the average current density (dashed line), $i = I_{st}/A_{fc}$, that is used to calculate the molar flow gradients in the GDL next to the catalyst. The solid line in the same subplot corresponds to the calculated apparent current density, i_{app}, in (24) based on the apparent area (25) that is not blocked by the liquid water film. Since these plots of current density were equivalent to the bond graph model output, the bond graph plots are omitted.

Subplot 2 shows the experimentally measured cell voltages [1] for all 24 cells in the stack (thin lines) and the predicted model voltage (thick line).

The next step is to begin an *Activity* analysis. It is important to reiterate that *Activity* results are highly dependent upon

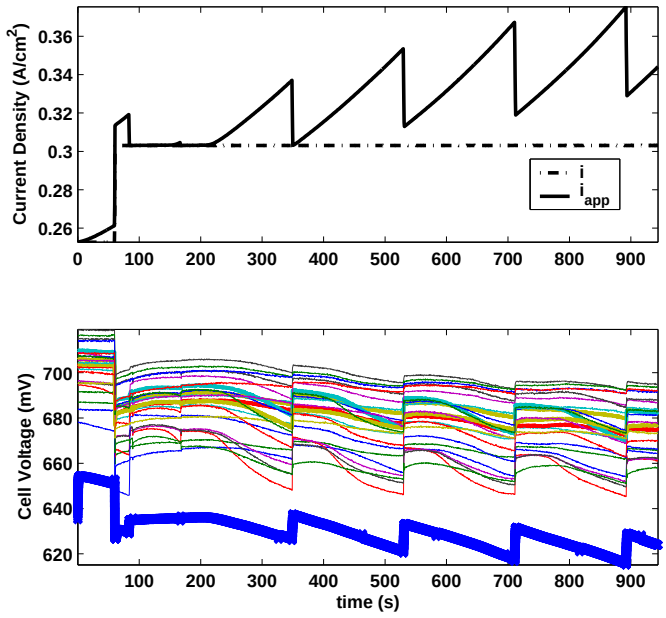

Figure 6. Measurements and model outputs for an experiment exhibiting anode flooding. The thin voltage lines correspond to the measured voltages, the thick line is the model prediction

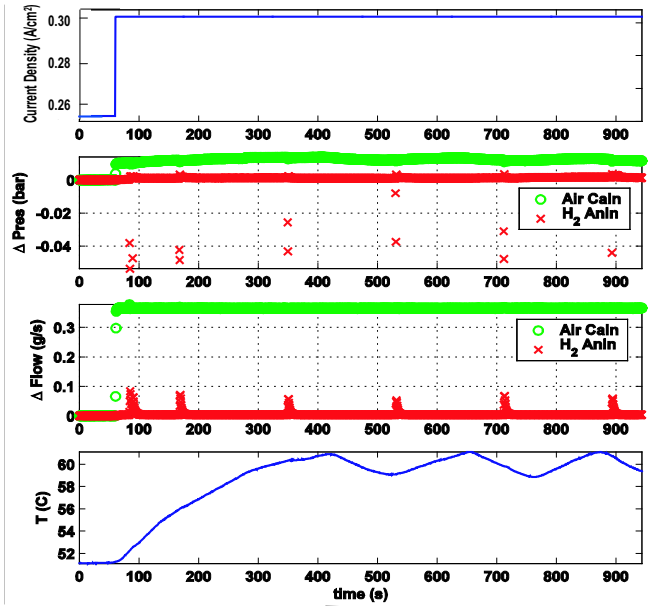

Figure 7. Measurements and model inputs for an experiment exhibiting anode flooding.

the duration of the simulation and the inputs to the system. For example, taking the time period to start immediately before a step current load is requested, and to end shortly thereafter would generate results highly dependent upon transient response, which would be quite different from results where the period is chosen to be 1000 sec straddling the same load request. Further, the *Activity Index*(AI) strongly depends upon what the modeler considers the content of the overall model to be. For example, exclusion of flow sources would have a profound effect on the *Activity* indices by changing the value for the *Total Activity* $(\sum_1^m Activity_i)$ of (2).

For this case study, the duration and inputs from [1] are used. In order to numerically obtain the system *Activity*, the model shown in Fig. 5 was simulated for 900 sec, using a temperature input that varied sinusoidally (period of 400 sec, amplitude of 2 °C), and a current density requirement that started at 0.25 A/cm^2, and stepped up to 0.30 A/cm^2 in 2 sec at time t=60 sec, as shown in Fig. 7. Further, anode channel purges were performed per Fig. 7, as well. Outputs of interest are the liquid water volumes in all sections of the model, the apparent current density, and the *Activity* of all elements and sources.

The *Activity* results, taken at the end of the calculation period (t = 900 sec), are normalized into percentages and listed in Table 1. The first aspect to notice is that the activities of the two water phases are significantly different in magnitude. The liquid water phase *Activities* are much smaller than those of the gas phase. This is caused by the low values of the volumetric flow rate. While both regimes have power that can be related to Joules, the power that results from liquid volumetric flow rate in (m^3/s), multiplied by capillary pressure is extremely low compared to the product of gaseous phase concentration and molar flow.

Table 1. Activities

Cathode Element	%Tot Activity	Anode Element	%Tot Activity
O_2 Diff sec1	0.410%	H_2 Diff sec1	0.434%
O_2 Diff sec2	0.410%	H_2 Diff sec2	0.433%
O_2 Diff sec3	0.406%	H_2 Diff sec3	0.434%
O_2 Conc sec1	0.001%	H_2 Conc sec1	0.062%
O_2 Conc sec2	0.001%	H_2 Conc sec2	0.063%
O_2 Conc sec3	0.001%	H_2 Conc sec3	0.063%
H_2O Diff sec1	0.211%	H_2O Diff sec1	0.011%
H_2O Diff sec2	0.506%	H_2O Diff sec2	0.011%
H_2O Diff sec3	0.476%	H_2O Diff sec3	0.110%
H_2O Conc sec1	0.003%	H_2O Conc sec1	0.002%
H_2O Conc sec2	0.003%	H_2O Conc sec2	0.002%
H_2O Conc sec3	0.003%	H_2O Conc sec3	0.003%
Liq Flow sec1	0.0002%	Liq Flow sec1	0.0001%
Liq Flow sec2	0.0008%	Liq Flow sec2	0.0002%
Liq Flow sec3	0.0080%	Liq Flow sec3	0.0004%
Liq p_{cap} sec1	0.0001%	Liq p_{cap} sec1	0.0001%
Liq p_{cap} sec2	0.0001%	Liq p_{cap} sec2	0.0001%
Liq p_{cap} sec3	0.0002%	Liq p_{cap} sec3	0.0001%

The reason that the *Activity* percentages shown in Table 1 do not total 100 is that all the source elements have not been listed as they are not under consideration for reduction at this time. Not surprisingly, the vast majority of the *Activity* in this system is taking place at the sources representing the gas flow inlets and

evaporation sites.

In an *Activity* analysis, it is common to compare *Activity* magnitudes, and conclude that either an element is negligible and can be eliminated, or that it's dynamics are fast enough to justify assignment of instantaneous equilibrium. A common threshold for such considerations is $< 0.1\%$. If we were to accept this limit for our application, it would appear that all the liquid water elements, and all of the capacitance elements, might be removed! As the point of the model is to predict liquid water dynamics, this direction is ill-suited to our case.

A key point to remember is that the goal of this reduction is to determine the sufficient level of discretization. Therefore, this application will use the *Activity* to determine how many sections are required. With this view, comparing the *Activity* levels, it can be seen that some species have very little *Activity* variation from section to section. It is assumed that small variation in activity implies *over-discretization*. Following this interpretation, the species listed in Table 2 have high potential for reduction.

Table 2. Candidate elements for reduction based upon similar Activities

Element	Element
O_2 Diff	H_2 Diff
O_2 Conc	H_2 Conc
H_2O Conc (Ca)	H_2O Conc (An)
Liq p_{cap} (Ca)	Liq p_{cap} Conc (An)

Lumping the diffusion equations (series resistances) together, and summing the capacitances (rate of change of concentration of gases), it proved to be true that the O_2 and H_2 gas flow modeling require, at most, just one section. Similar results were found for the anode side liquid dynamics. Reducing these sections to a single larger section had no effect on the modeled liquid water volume reaching the anode channel. The H_2O vapor may not be reducible to one section due to the spatial variation in *Activity* for the associated diffusion. These reductions eliminate over 20% of the model equations and states, reducing the 25 state model to one with 19 states.

8 Conclusions

A bond graph model of a three-section anode GDL and three-section cathode GDL has been created and verified. The model was used to apply a model order reduction technique known as MORA, which is an energy-based reduction method that preserves physical variables and parameters. The complexity of the model was reduced by over 20%, with significant further reduction likely. MORA was used to determine the appropriate level of discretization by considering a lack of *Activity* variation from section-to-section as indicative of an opportunity to reduce the number of sections for that species. The bond graph model will be useful for future investigations on model complexity, as well as for sensitivity studies.

9 Future Work

Further study into the application of model-order reduction will focus on the influence of the critical *time duration*, including the relation to the various time constants of the system. Subsequent research is expected on the topic of water distribution within the gas flow channel.

REFERENCES

[1] McKay, D. A., Ott, W. T., and Stefanopoulou, A. G., 2005. "Modeling, parameter identification, and validation of water dynamics for a fuel cell stack". ASME Conference on Fuel Cell Science, Engineering and Technology. FUELCELL2005-81484.

[2] Louca, L., Stein, J., Hulbert, G., and Sprague, J., 1997. "Proper model generation: An energy-based methodology". *Proceedings of the 1997 International Conference on Bond Graph Modeling*, p. 44.

[3] Yi, J., and Nguyen, T., 1998. "An along the channel model for proton exchange membrane fuel cells". *Journal of the Electrochemical Society*.

[4] Fuller, T., and Newman, J., 1993. "Water and thermal management in solid-polymer-electrolyte fuel cells". *Journal of the Electrochemical Society*.

[5] Dutta, S., and Shimpalee, S., 2001. "Numerical prediction of mass-exchange between cathode and anode channels in a pem fuel cell". *International Journal of Heat and Mass Transfer*.

[6] Pasaogullari, U., and Wang, C.-Y., 2005. "Two-phase modeling and flooding prediction of polymer electrolyte fuel cells". *Journal of The Electrochemical Society*.

[7] Nam, J. H., and Kaviany, M. "Effective diffusivity and water-saturation distribution in single- and two-layer pemfc diffusion medium". *Int. J Heat Mass Transfer*, **46**, p. 4595.

[8] Springer, T., Zawodzinski, T., and Gottesfeld, S., 1991. "Polymer electrolyte fuel cell model". *Journal of the Electrochemical Society*.